Hyaluronic Acid–Gold Nanoparticle/Interferon α Complex for Targeted Treatment of Hepatitis C Virus Infection

Min-Young Lee,[†] Jeong-A Yang,[†] Ho Sang Jung,[†] Songeun Beack,[†] Jung Eun Choi,[‡] Wonhee Hur,[‡] Heebeom Koo,[§] Kwangmeyung Kim,[§] Seung Kew Yoon,[‡] and Sei Kwang Hahn[†,*]

[†]Department of Materials Science and Engineering, Pohang University of Science and Technology (POSTECH), San 31, Hyoja-dong, Nam-gu, Pohang, Kyungbuk 790-784, Korea, [‡]Department of Internal Medicine and WHO Collaborating Center of Viral Hepatitis, The Catholic University of Korea, 505 Banpo-dong, Seocho-gu, Seoul 137-701, Korea, and [§]Center for Theragnosis, Biomedical Research Institute, Korea Institute of Science and Technology, 39-1 Hawolgok-dong, Seongbuk-gu, Seoul 136-791, Korea

ABSTRACT Gold nanoparticles (AuNPs) have been extensively investigated as an emerging delivery carrier of various biopharmaceuticals. Instead of nonspecific polyethylene glycol (PEG) conjugated interferon α (IFNα) for the clinical treatment of hepatitis C virus (HCV) infection, in this work, a target-specific long-acting delivery system of IFNα was successfully developed using the hybrid materials of AuNP and hyaluronic acid (HA). The HA–AuNP/IFNα complex was prepared by chemical binding of thiolated HA and physical binding of IFNα to AuNP. According to antiproliferation tests in Daudi cells, the HA–AuNP/IFNα complex showed a comparable biological activity to PEG-Intron with a highly enhanced stability in human serum. Even 7 days postinjection, HA–AuNP/IFNα complex was target-specifically delivered and remained in the murine liver tissue, whereas IFNα and PEG-Intron were not detected in the liver. Accordingly, HA–AuNP/IFNα complex significantly enhanced the expression of 2′,5′-oligoadenylate synthetase 1 (OAS1) for innate immune responses to viral infection in the liver tissue, which was much higher than those by IFNα, PEG-Intron, and AuNP/IFNα complex. Taken together, the target-specific HA–AuNP/IFNα complex was thought to be successfully applied to the systemic treatment of HCV infection.

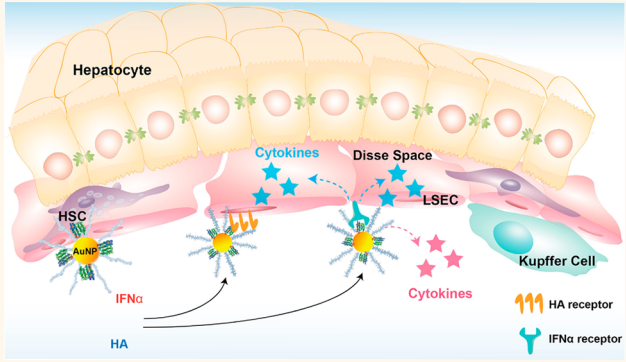

KEYWORDS: gold nanoparticle · hyaluronic acid · interferon α · targeted delivery · hepatitis C virus

Gold nanoparticles (AuNPs) have been exploited for various biomedical applications as a biocompatible carrier of biopharmaceuticals, a contrast agent for diagnostic imaging, and a photoabsorber for photothermal therapy.[1−4] AuNPs have many advantages such as biocompatibility, simple synthesis, facile surface modification, versatile conjugation with biomolecules, and tunable optical properties.[4,5] Recently, AuNPs have been widely investigated as a nanocarrier of protein drugs. Rotello *et al.* reported a cationic tetra-alkyl ammonium-functionalized AuNP/anionic protein complex *via* electrostatic interaction, whose activity was maintained after releasing from the AuNP/protein complex by treatment with glutathione (GSH).[6] Chou *et al.* have also demonstrated that fluorescent gold nanoclusters with insulin have preserved the bioactivity of insulin, providing a versatility for cellular imaging.[7] In addition, Tamarkin *et al.* reported AuNP conjugated with thiolated polyethylene glycols (PEGs) tethering tumor necrosis factors (TNFs), which is now in phase III clinical tests under the trade name AurImmune.[8,9] The technical barriers of systemically administered nanoparticle-based protein drug delivery systems are known to be the uptake by the reticuloendothelial system (RES) and macrophages, renal and biliary clearance, and enzymatic degradation of the protein in the body.[10,11]

As a drug delivery carrier, a biocompatible linear polysaccharide of hyaluronic acid

* Address correspondence to skhanb@postech.ac.kr.

Received for review June 8, 2012 and accepted October 24, 2012.

Published online October 24, 2012
10.1021/nn302538y

(HA)[10] has several advantages such as antifouling effect on the prevention of protein adsorption and opsonization, due to its hydrophilic and polyanionic characteristics in physiological environment,[11−13] and highly efficient targeted delivery to liver tissues with HA receptors such as hyaluronan receptor for endocytosis (HARE) and cluster determinant 44 (CD44).[14−16] HA derivatives with a modification degree less than *ca.* 25 mol % were specifically delivered to the liver and remained much longer in cirrhotic mice than normal mice.[17] In addition, they were more efficiently delivered to hepatic stellate cells (HSCs) and hepatoma cells than normal hepatocytes.[17] On the basis of these findings, we developed a target-specific HA−interferon α (IFNα) conjugate as an alternative to nonspecific PEGylated IFNα such as PEGASYS and PEG-Intron for the treatment of hepatitis C virus (HCV) infection.[18] The sustained virological response (SVR) rates of chronic HCV patients treated with PEGASYS and PEG-Intron were only 39% and 23% with a side effect after repeated injections possibly due to the nonspecific delivery by PEGylation.[19,20] However, the HA−IFNα conjugate was target-specifically delivered to the liver and induced higher expression of 2′,5′-oligoadenylate synthetase 1 (OAS1) than that of PEG-Intron 3 days postinjection.

In this work, we developed a new target-specific delivery system of IFNα using hybrid materials of AuNP and HA to improve the efficacy of IFNα for the treatment of chronic HCV infection. We found that IFNα tightly bound to AuNP and remained on the surface of AuNP at the physiological pH of 7.4 even after repeated centrifugation and extensive washing. For target-specific delivery, we introduced HA to the AuNP/IFNα complex system to prepare a HA−AuNP/IFNα complex. HA−AuNP/IFNα complex was characterized by ELISA, UV−vis spectra, dynamic light scattering (DLS), transmission electron microscopy (TEM), and circular dichroism (CD) spectroscopy. After confirmation of *in vitro* antiproliferation activity and serum stability in Daudi cells, target-specific systemic delivery of HA−AuNP/IFNα complex was carried out for the treatment of chronic HCV infection. *In vivo* antiviral activity of HA−AuNP/IFNα complex was assessed by measuring the expression levels of OAS1, which is induced by IFNα and participates in innate immune responses to viral infection in the liver.[21] The target-specific delivery system of HA−AuNP/IFNα complex was discussed for further clinical applications for the treatment of various liver diseases.

RESULTS AND DISCUSSION

Preparation of HA−AuNP/IFNα Complex. Figure 1a shows a strategic illustration of HA−AuNP/IFNα complex for the targeted systemic treatment of HCV infection. In our previous work, real-time bioimaging of HA derivatives using quantum dots revealed that HA derivatives could be target-specifically delivered to liver sinusoidal endothelial cells (LSECs) and HSCs.[17] HSCs have a less contacting chance with HA in the blood because HSCs exist under the LSEC layer in a normal liver. However, the more seriously liver disease has progressed, the more HSCs are activated.[17] It has been reported that HSCs in cirrhotic liver proliferated by 10−20 times and squeezed through the LSEC fenestrae.[22] Accordingly, we hypothesized that HA−AuNP/IFNα complex can bind to HA receptor and IFNα receptor on the surface of mainly LSECs or HSCs by a dual targeting effect promoting IFNα-induced cytokine release. The IFNα-induced cytokine can affect the hepatocyte in the neighborhood by paracrine signaling, which is one of the cell signaling forms to target cells near the signal-releaseing cells.[23] Figure 1b shows a schematic representation of the preparation of the HA−AuNP/IFNα complex. First, thiol end-functionalized HA (HA−SH) was synthesized by reductive amination of HA with cystamine and then reduction with DTT as described elsewhere.[24] The obtained HA−SH was immobilized onto the surface of AuNP *via* gold−thiol chemistry. The size of the AuNP was *ca.* 22.16 nm with a narrow PDI of 0.14 according to the DLS analysis. Then, IFNα was mixed with HA−AuNP (or AuNP) at pH 7.4. The unbound HA and IFNα were removed by repeated centrifugation and washing. The average number of HA molecules bound to a single AuNP was *ca.* 70. The number of IFNα molecules added per single HA−AuNP for the preparation of HA−AuNP/IFNα complex was 10, 20, 50, 100, and 200, respectively. With increasing feed ratio of IFNα to single HA−AuNP, the protein content bound to the HA−AuNP increased up to *ca.* 110, covering all of the available binding sites with IFNα. The IFNα content in HA−AuNP/IFNα (or AuNP/IFNα) complex was determined by ELISA. The maximal number of IFNα per AuNP without HA was *ca.* 120, and the complex was described as AuNP/IFNα 120 complex. To confirm the IFNα content in HA−AuNP/IFNα (or AuNP/IFNα) complex, we prepared FITC-labeled IFNα and compared the amount of FITC-IFNα in the supernatant and in the HA−AuNP/IFNα complex after etching the AuNPs with 0.2 M KCN. The results were well matched with those by the ELISA assay (Figure S1). While AuNP and AuNP/IFNα 17 complex were gradually aggregated and precipitated in a NaCl solution (150 mM) AuNP/IFNα 120 complex remained stable for up to 24 h (Figure S2). In addition, HA−AuNP and all of the HA−AuNP/IFNα complexes were very stable in a high ionic strength NaCl solution (150 mM) without aggregation and precipitation for up to 24 h.

Characterization of HA−AuNP/IFNα Complex. The formation of AuNP/IFNα and HA−AuNP/IFNα complexes was assessed by UV−vis spectra, DLS, and TEM. The direct interaction of IFNα with AuNP was confirmed from the red shift in the surface plasmon resonance (SPR) band of AuNP after addition of IFNα. The SPR peak of free AuNP appeared around 519 nm and that of

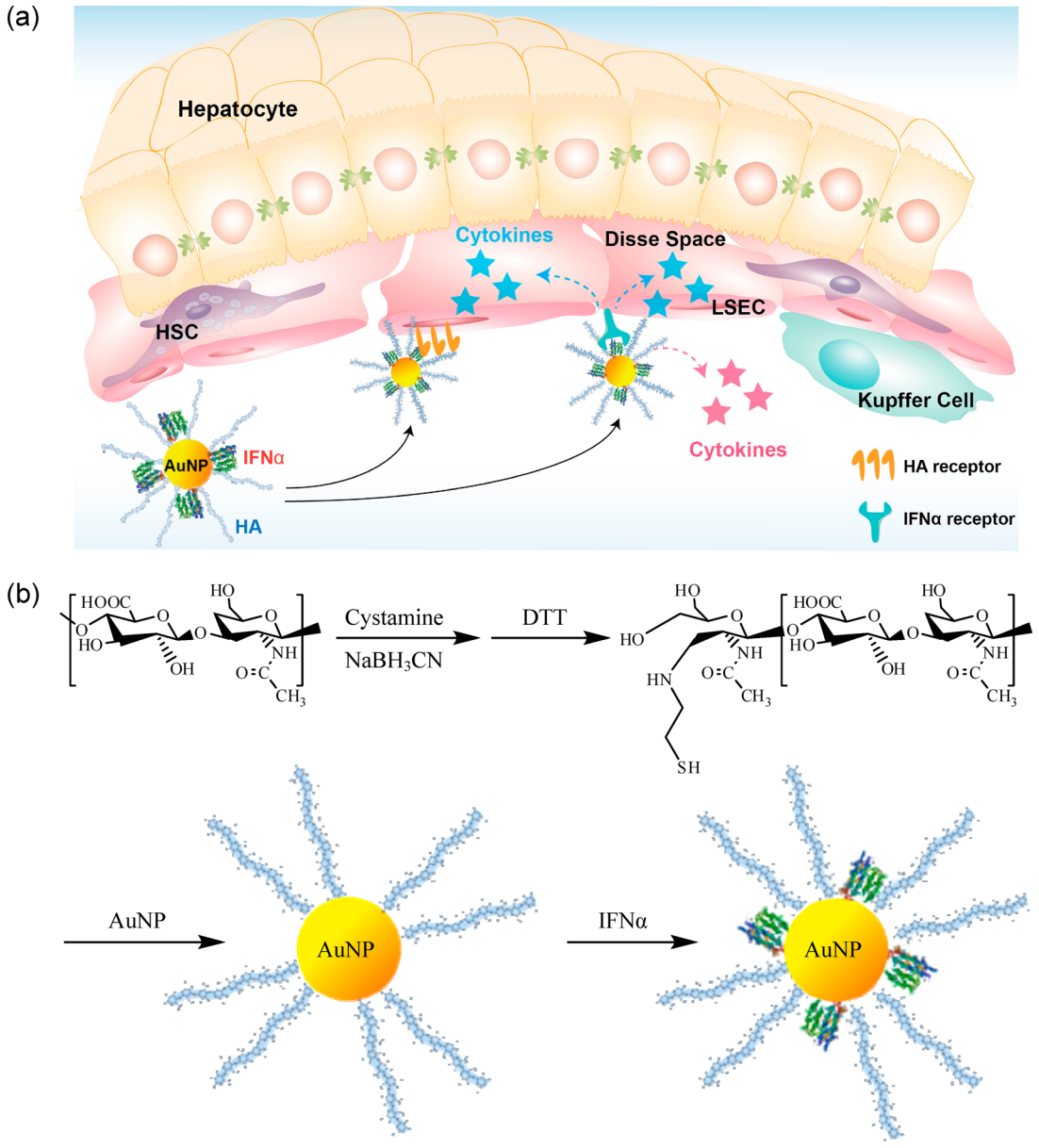

Figure 1. (a) Strategic illustration of HA–AuNP/IFNα complex for the target-specific systemic treatment of HCV infection. (b) Schematic representations for the preparation of thiol end-modified HA and HA–AuNP/IFNα complex.

AuNP/IFNα complex was shifted to 526 nm (Figure 2a). The stepwise binding of HA-SH and IFNα to AuNP shifted the SPR peak to 523 and 527 nm, respectively (Figure 2b). After binding IFNα, the mean hydrodynamic diameter of AuNPs increased from 22.16 nm with a PDI of 0.142 to 29.25 nm with a PDI of 0.164 (Figure 3a). The difference of the diameter between free AuNP and AuNP/IFNα complex was *ca.* 7 nm, reflecting a single-layer binding of IFNα with a dimension of *ca.* 3–4 nm to AuNP without aggregation.[25,26] The mean hydrodynamic diameters of HA–AuNP and HA–AuNP/IFNα complex were 46.03 nm with a PDI of 0.099 and 52.23 nm with a PDI of 0.089, respectively. TEM images in Figure 3b and c exhibited the monodispersed morphology of AuNP/IFNα and HA–AuNP/IFNα complexes.

To investigate the mechanism for the formation of HA–AuNP/IFNα (or AuNP/IFNα) complex, we tried to release the protein from the surface of AuNP by disrupting the specific interactions. As reported elsewhere,[25] proteins can physically bind onto the surface of AuNPs by electrostatic attraction and/or hydro phobic interaction, as well as covalent bonding. HA–AuNP/IFNα (AuNP/IFNα) complex was incubated in either a high ionic strength solution (1 M $MgCl_2$) or a detergent solution (1% Tween 20). After incubation for 3 h and centrifugation, the supernatant was analyzed by ELISA. As shown in Figure S3, the amount of released IFNα from the HA–AuNP/IFNα complex was 10.1% in a $MgCl_2$ solution and 42.6% in a Tween 20 solution. The hydrophobic interaction appeared to contribute more than the electrostatic attraction for

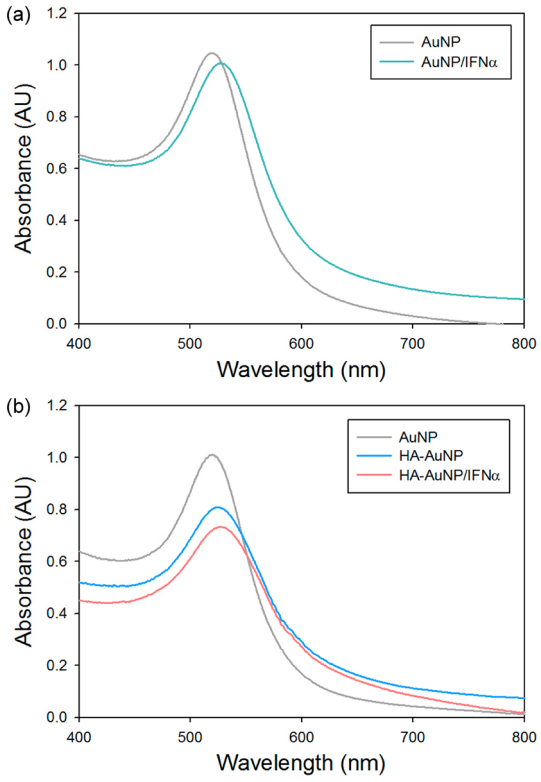

Figure 2. UV–vis spectra of (a) AuNP/IFNα and (b) HA–AuNP/IFNα complexes.

the binding of IFNα onto AuNP. However, because 95.3% of IFNα was released from the HA–AuNP/IFNα complex in a $MgCl_2$ plus Tween 20 solution, IFNα was thought to bind the HA–AuNP by the synergistic combination of electrostatic and hydrophobic interactions. AuNP/IFNα complex also showed a similar trend. These results indicated that there was almost no chemical bonding between AuNP and thiols in IFNα. IFNα contains four cysteine residues that form two disulfide bonds playing an important role in its biological activity.[28] Then, the stability of HA–AuNP/IFNα (AuNP/IFNα) complex by electrostatic and hydrophobic interactions was investigated in the serum. It was reported that blood proteins can interact with AuNP.[29] Especially, serum albumin is known to interact strongly with AuNP.[30] Although IFNα was gradually released from HA–AuNP/IFNα 17 complex in bovine serum albumin (BSA) solution with increasing time, the amount of released IFNα from AuNP/IFNα 120, HA–AuNP/IFNα 75, and HA–AuNP/IFNα 110 complexes was very low for up to 3 days (Figure S4). The HA–AuNP/IFNα complex with the higher IFNα content was more stable in BSA solution, preventing the binding of BSA onto AuNPs.

The secondary structure of IFNα was analyzed by CD spectroscopy before and after being released from the HA–AuNP/IFNα complex (Figure 4). IFNα displayed the characteristic CD spectra with a negative ellipticity peak at 208 and 220 nm, indicating an α-helical structure. The achiral HA–AuNP (or AuNP) had a noisy spectrum without a UV–vis CD response at 200–250 nm. After binding of IFNα to the surface of HA–AuNP, HA–AuNP/IFNα complex showed a clear change in the UV–vis CD spectrum, reflecting the conformational change of IFNα and/or energy transfer from the protein to the AuNP (Figure 4a).[31] For further investigation, CD analysis was carried out for the IFNα released from the HA–AuNP/IFNα complex (Figure 4b). The CD spectrum of the native IFNα was not changed in the $MgCl_2$ plus Tween 20 solution. In addition, the CD spectrum of IFNα released from the HA–AuNP/IFNα complex was identical to that of the native IFNα, which revealed that the secondary structure of IFNα was maintained after binding onto the surface of HA–AuNP. From the results, the energy transfer from the protein to the AuNP was thought to be the main reason for the CD spectral change after binding of IFNα to HA–AuNP.

***In Vitro* Biological Activity of HA–AuNP/IFNα Complex.** *In vitro* biological activity of AuNP-based IFNα complexes was investigated by an antiproliferation assay of Daudi cells with increasing concentration of IFNα. Daudi cells, human B-lymphoblasts, are very sensitive to IFNα and arrested in the G0/G1 phase of the cell cycle in the presence of IFNα.[32] Accordingly, their growth is inhibited in the presence of a very low concentration of IFNα. Before the antiproliferation assay, the cytocompatibility of HA–AuNP was assessed in Daudi cells by the MTS assay. There was no significant effect on the proliferation or cell viability, even when the concentration of HA–AuNP was 10 times higher than that for the biological activity test of HA–AuNP/IFNα complex (Figure S5). Then, the antiproliferation activity of AuNP/IFNα 120, HA–AuNP/IFNα 75, and HA–AuNP/IFNα 110 complexes was compared with that of IFNα and PEG-Intron by measuring the concentration for 50% inhibition of cell growth (IC_{50}) (Figure 5a). The antiproliferation effect of AuNP-based IFNα complexes was lower than that of native IFNα, but comparable to that of PEG-Intron. Because IFNα was slowly released from the complexes in the physiological environment, the biological activity of AuNP-based IFNα complexes might be enhanced after release in the body. To investigate the direct serum stability of AuNP-based IFNα complexes, native IFNα and AuNP-based IFNα complexes were incubated in human serum at 37 °C for 4 days and assessed for the biological activity of IFNα as described above. As shown in Figure 5b, IFNα degraded in human serum, and the biological activity was reduced to one-twentieth compared with that of native IFNα. On the other hand, AuNP/IFNα 120, HA–AuNP/IFNα 75, and HA–AuNP/IFNα 110 complexes showed a serum stability, maintaining bioactivity for up to 4 days in human serum. The AuNP-based IFNα complexes with enhanced serum stability might be beneficial for the systemic treatment of liver diseases such as chronic HCV infection and liver cancer.

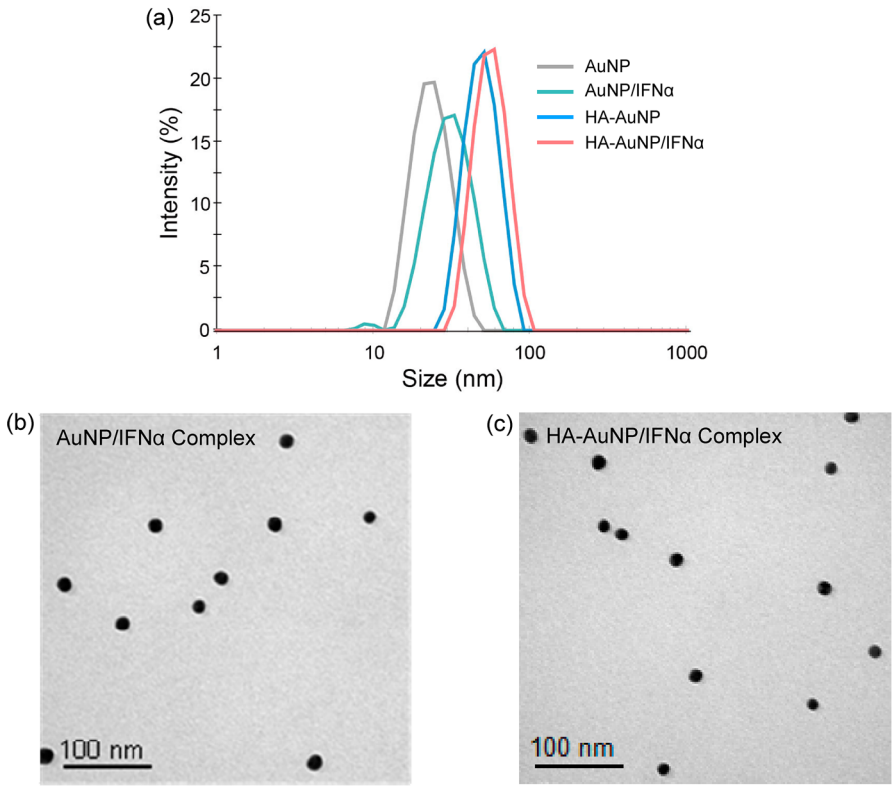

Figure 3. (a) Dynamic light scattering analysis for the hydrodynamic diameter of AuNP/IFNα and HA−AuNP/IFNα complexes. Transmission electron microscopic images of (b) AuNP/IFNα and (c) HA−AuNP/IFNα complexes.

***In Vivo* Distribution of HA−AuNP/IFNα Complex.** For an *in vivo* body distribution study of the HA−AuNP/IFNα complex, the accumulation in the liver tissue was first investigated by human IFNα ELISA 4 h and 1, 3, and 7 days after a single intravenous injection of six kinds of samples: PBS, IFNα, PEG-Intron, HA-AuNP, AuNP/IFNα 120, and HA−AuNP/IFNα 110 complexes (Figure 6). HA−AuNP did not show any effect on the IFNα concentration in the liver tissue. Native IFNα was detected at a very low level of *ca.* 15 pg/(mg protein) in the liver tissue after 4 h and was not detected 1, 3, and 7 days postinjection due to the rapid clearance within 24 h in the body.[18] In the case of PEG-Intron, IFNα was detected at a higher level than native IFNα until 3 days, but was not detected at 7 days. Interestingly, the amount of IFNα in HA−AuNP/IFNα 110 complex accumulated in the liver was much higher than that of PEG-Intron remaining even after 7 days. The IFNα in AuNP/IFNα 120 complex was also detected at 7 days, but the total amount was significantly lower than that of HA−AuNP/IFNα 110 complex. Then, the hepatocellular distribution of HA−AuNP/IFNα 110 complex was investigated in Balb/c mice. Parenchymal (PC, hepatocytes) and non-parenchymal (Kupffer cells, LSECs, and HSCs) cells were isolated from the liver by the collagenase perfusion two-step method. The cell-specific distribution of AuNP-based IFNα complexes was analyzed by ICP-MS. The distribution of HA−AuNP/IFNα 110 complex was the highest at *ca.* 1411 fg/cell in LSEC, followed by *ca.* 120 fg/cell in PC *via* fenestrae, and *ca.* 4 fg/cell in other cells, respectively (Figure S6). HA−AuNP showed a similar trend with HA−AuNP/IFNα 110 complex on the hepatocellular distribution. In contrast, the distribution of AuNP/IFNα 120 complex was only *ca.* 374 fg/cell in LSEC, *ca.* 14 fg/cell in PC, and *ca.* 150 fg/cell in other cells including Kupffer cells. TEM clearly visualized the well-dispersed HA−AuNP/IFNα 110 complexes taken up in LSECs (Figure 7). The results are well matched with our previous report on target-specific delivery of HA derivatives to liver tissues including LSECs and HSCs.[17]

On the basis of the hepatocellular distribution time profile, the distribution of HA−AuNP/IFNα complex in major organs was investigated 1 day after the single injection in comparison with AuNP/IFNα 120 complex (Figure 8). The IFNα level of HA−AuNP/IFNα 110 complex was the highest at *ca.* 236 pg/(mg proteins) in the liver, followed by *ca.* 120 pg/(mg proteins) in the spleen, *ca.* 11 pg/(mg proteins) in the kidney, and no detection in the lung (Figure 8a). However, the IFNα level of AuNP/IFNα 120 complex was the highest at *ca.* 128 pg/(mg proteins) in the spleen, followed by *ca.* 98 pg/(mg proteins) in the liver, *ca.* 50 pg/(mg proteins) in the lung, and *ca.* 16 pg/(mg proteins) in the kidney. The analysis of Au content in these organs by ICP-MS also showed a similar trend 1 day postinjection of AuNP/IFNα 120 and HA−AuNP/IFN 110 complexes (Figure 8b). There have been many reports on severe lung toxicity after IFNα monotherapy as well as combination therapies with

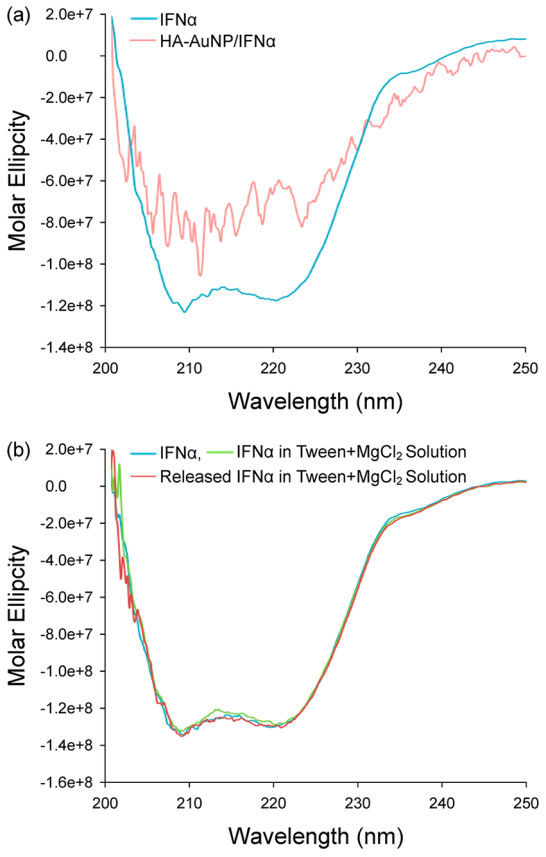

Figure 4. Circular dichroism spectra of (a) IFNα and HA−AuNP/IFNα complex and (b) released IFNα from HA−AuNP/IFNα complex in a Tween 20 plus $MgCl_2$ solution.

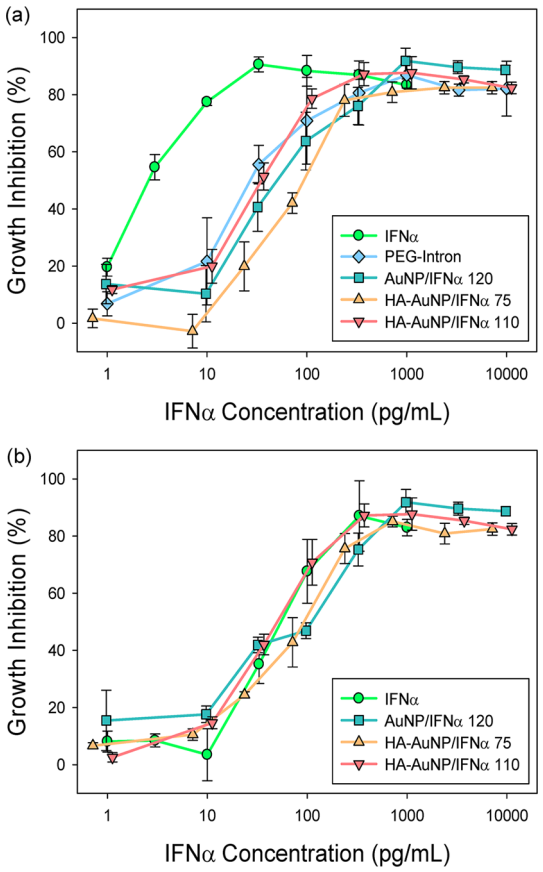

Figure 5. (a) *In vitro* antiproliferation activity of AuNP-based IFNα complexes compared with native IFNα and PEG-Intron in Daudi cells (n = 3). (b) *In vitro* antiproliferation activity of AuNP-based IFNα complexes and IFNα after incubation in human serum at 37 °C for 4 days (n = 3).

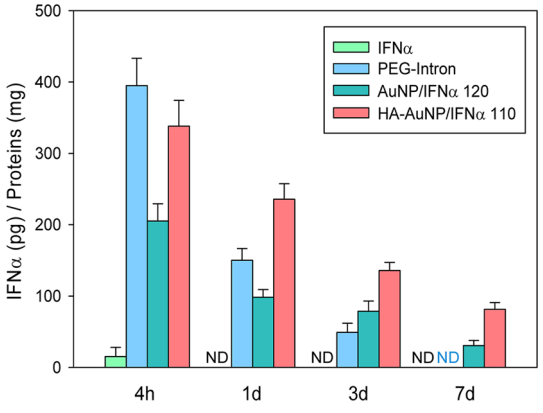

Figure 6. IFNα content accumulated in the liver tissue 4 h and 1, 3, and 7 days after intravenous injection of native IFNα, PEG-Intron, AuNP/IFNα 120, and HA−AuNP/IFNα 110 complexes (n = 3, ND = no detection).

Ribavirin and conventional or PEGylated IFNα, such as interstitial pneumonia, bronchiolitis obliterans organizing pneumonia (BOOP), sarcoidosis, and severe profiles of asthma exacerbation.[33] In contrast, HA might be highly efficient for target-specific delivery of drugs to the liver tissues with HA receptors reducing the side effects.[12−18] In addition, polyanionic HA has the antifouling effect preventing protein adsorption and opsonization, and prohibits enzymatic degradation of IFNα *via* steric hindrance. Nanoparticles larger than 10 nm were reported to avoid rapid clearance *via* renal filtration and urinary excretion.[10] Therefore, HA−AuNP/IFNα 110 complex might be more advantageous than the conventional or PEGylated IFNα with minimal side effects.

***In Vivo* Antiviral Activity of HA−AuNP/IFNα Complex.** OAS1 is expressed by IFNα stimulation and is one of the key components for the innate immune responses to HCV infection.[21] OAS1 initiates the synthesis of 2′,5′-oligoadenylate, which activates the RNase L-associated pathway leading to the cleavage of viral and cellular RNAs.[34] The antiviral activity of IFNα is highly related with OAS1 expression level, which is widely used to predict the sustained viral response and therapeutic effect of interferon-based treatment on chronic HCV infection.[21] We monitored the OAS1 expression levels in the liver tissue 7 days after intravenous injection of PBS as a control, IFNα, PEG-Intron, HA−AuNP, AuNP/IFNα 120, HA−AuNP/IFNα 75, and HA−AuNP/IFNα 110 complexes (Figure 9). The elevated OAS1 expression level by treatment with AuNP/IFNα and HA−AuNP/IFNα complexes was more significant than those by native IFNα and PEG-Intron (Figure 9a). According to the densitometric quantification of Western blots, HA−AuNP/IFNα 110 complex

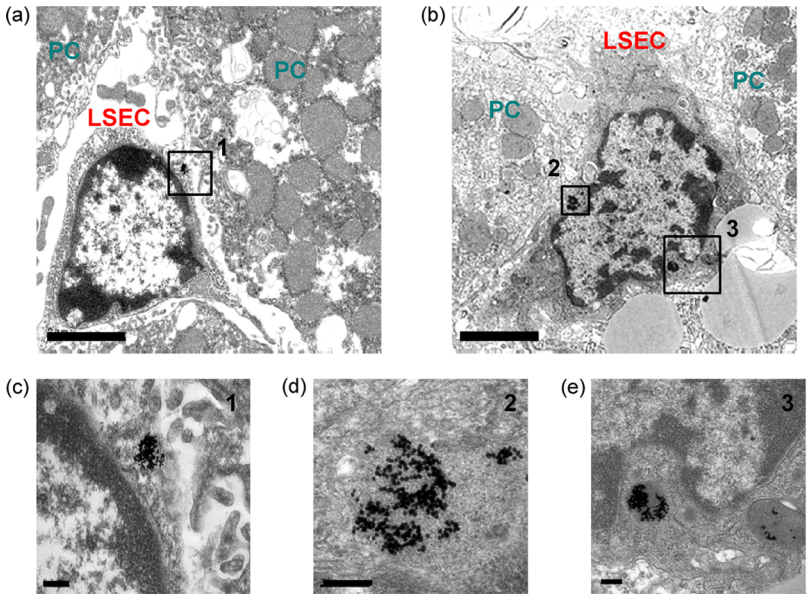

Figure 7. Transmission electron micrographs of HA−AuNP/IFNα 110 complex (a, b) in two representative LSECs between parenchymal cells in the liver tissue and (c, d, e) their magnified images in the regions 1, 2, and 3. Scale bars indicate 2 μm in (a, b) and 200 nm in (c, d, e).

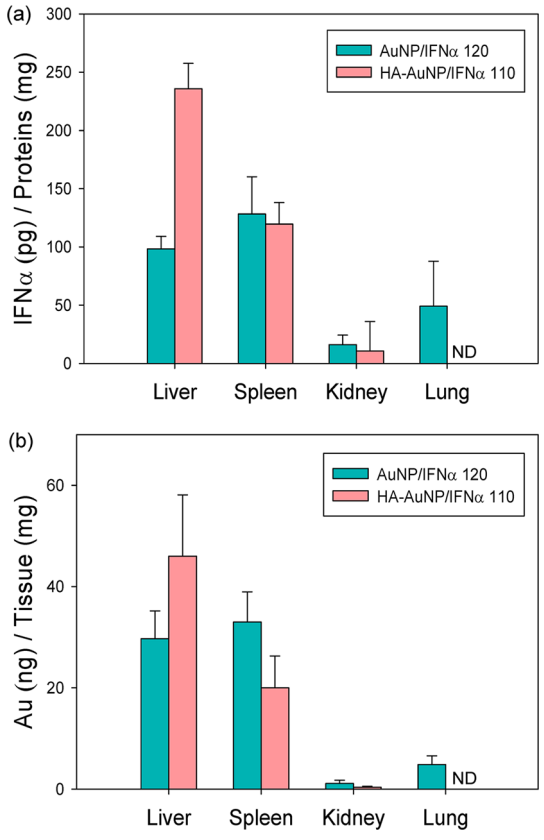

Figure 8. (a) IFNα content and (b) Au content in major organs of mice 1 day after intravenous injection of AuNP/IFNα 120 and HA−AuNP/IFNα 110 complexes (n = 3).

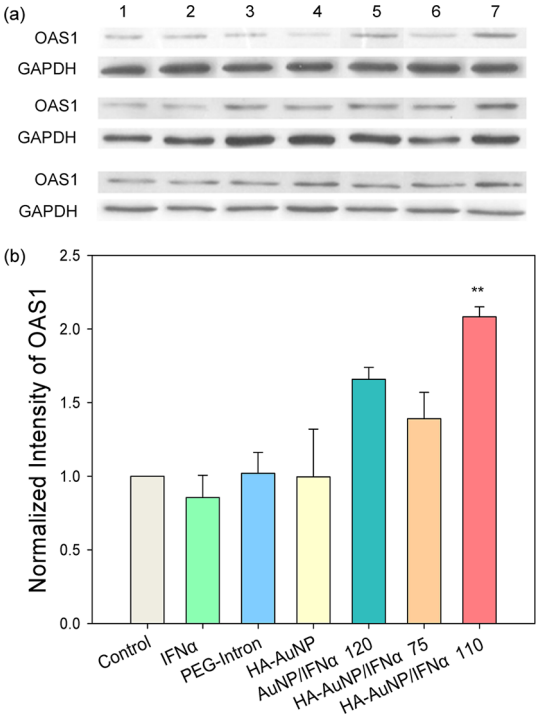

Figure 9. (a) Western blot analysis of OAS1 in mouse liver tissues 7 days after intravenous injection of (1) PBS as a control, (2) native IFNα, (3) PEG-Intron, (4) HA−AuNP, (5) AuNP/IFNα 120, (6) HA−AuNP/IFNα 75, and (7) HA−AuNP/IFNα 110 complexes. (b) Quantification of the expressed OAS1 level by densitometric analysis (n = 3). **p < 0.01 *versus* AuNP/IFNα 120 complex.

enhanced the OAS1 level statistically higher than HA−AuNP/IFNα 75 and AuNP/IFNα 120 complexes (Figure 9b). The relatively high expression of OAS1 by the treatment with HA−AuNP/IFNα 110 complex might be attributed to the enhanced stability in the body and target-specific delivery of the complex to the liver tissue (Figure 6). HA−AuNP had no effect on OAS1 expression, indicating that the enhanced OAS1 expression was solely induced by the IFNα in the HA−AuNP/IFNα

complex. This prolonged and improved therapeutic effect for longer than 7 days confirmed the feasibility of HA−AuNP/IFNα 110 complex for the treatment of HCV infection. The target-specific HA−AuNP/IFNα complex might be successfully developed for further clinical applications. Moreover, the HA−AuNP was thought to be effectively exploited to prepare a diverse protein complex for target-specific systemic treatment of various liver diseases.

CONCLUSION

HA−AuNP/IFNα complex was successfully prepared by chemical binding of thiolated HA and physical binding of IFNα to AuNP. UV−vis spectra and DLS analyses confirmed the successful formation of HA−AuNP/IFNα complex. CD analysis revealed the maintenance of the secondary structure of IFNα even after binding to HA−AuNP. According to antiproliferation tests in Daudi cells, *in vitro* biological activity of HA−AuNP/IFNα complex was lower than that of native IFNα, but comparable to that of PEG-Intron. HA−AuNP/IFNα complex showed highly enhanced stability in human serum. After intravenous injection, HA−AuNP/IFNα complex was target-specifically delivered and remained in the liver tissue longer than 7 days. The normalized OAS1 expression levels in the liver tissues clearly demonstrated a more significant therapeutic effect of HA−AuNP/IFNα 110 complex even 7 days postinjection than native IFNα and PEG-Intron. The results might be attributed to the enhanced serum stability of HA−AuNP/IFNα complex and its target-specific delivery to the liver tissue. Taken together, HA−AuNP/IFNα complex was thought to have a great potential as a new nanomedicine with an enhanced and prolonged efficacy for the treatment of chronic HCV infection.

MATERIALS AND METHODS

Materials. Sodium hyaluronate, the sodium salt of hyaluronic acid, with a molecular weight of 12 kDa was purchased from Lifecore Co. (Chaska, MN, USA). Chloroauric acid ($HAuCl_4$), sodium citrate, tris(2-carboxyethyl)phosphine hydrochloride (TCEP-HCl), fluorescein isothiocyanate (FITC), 6′-aminofluorescein, and human serum were obtained from Sigma-Aldrich (St. Louis, MO, USA). The PD-10 desalting column was purchased from GE Healthcare (Uppsala, Sweden). Human interferon α-2b (IFNα-2b) and PEG-Intron were kindly provided by Shinpoong Pharmaceutical Co. (Seoul, Korea). Cell Titer 96 AQueous One Solution Reagent was purchased from Promega (Madison, WI, USA), and BCA protein assay kit from Thermo Scientific (Rockford, IL, USA). The human IFNα ELISA kit was purchased from PBL InterferonSource (Piscataway, NJ, USA). Human Daudi cell line was purchased from Korean Cell Line Bank. Rabbit anti-OAS1 polyclonal antibody and rabbit anti-glyceraldehyde 3-phosphate dehydrogenase (GAPHD) monoclonal antibody were obtained from Santa Cruz Biotechnology (Santa Cruz, CA, USA). Horseradish peroxidase-conjugated goat anti-rabbit IgG was purchased from Kirkegaard and Perry Laboratories (Gaithersburg, MD, USA). All procedures with animals were carried out in accordance with Pohang University of Science and Technology (POSTECH) guidelines for animal care and use. Deionized water was used in this work, and all reagents were used without further purification. The protein structures of IFNα and serum albumin in Figures 1 and S4 were obtained from DrugBank.

Synthesis of Thiol End-Modified HA. HA−SH was prepared by reductive amination as described elsewhere.[24] HA (MW 12 000, 100 mg) and cystamine dihydrochloride (60 mg) were dissolved in 0.1 M borate buffer (10 mL, pH 8.5) with 0.4 M NaCl and stirred for 2 h. $NaBH_3CN$ was added to the solution at a final concentration of 200 mM and reacted at 40 °C for 5 days. The reaction mixture was incubated with 100 mM DTT for 12 h to introdue a free thiol group, dialyzed (MWCO: 3500 Da) against a large excess of 100 mM NaCl solution for 2 days, 25% ethanol for 1 day, and pure water for 1 day to remove unreacted chemicals, and freeze-dried for 3 days. Before use, HA−SH was treated with TCEP to completely reduce disulfide bonds and eluted through PD-10 desalting column to remove TCEP. The efficiency of thiol end-functionalization of HA was higher than 95%, as determined by Ellman's assay.

Preparation of HA−AuNP/IFNα Complex. AuNPs were synthesized using citrate as a reducing agent and stabilizer. $HAuCl_4$ (10 mg) was dissolved in 90 mL of water, and the solution was heated to boiling. Sodium citrate solution (500 μL of 250 mM) was added to the boiling solution and stirred for 30 min until the color turned to wine-red. HA−SH solution (820 μL of 1 mg/mL) was added to the AuNP solution (50 mL of 5.4 nM), which was stirred for 24 h. HA−AuNP was purified by centrifugation at 20000*g* for 20 min and redispersed in water (pH 7.4). The average number of HA molecules bound to a single AuNP was determined by measuring the fluorescence intensity of aminofluorescein-labeled HA after etching the AuNPs in 0.2 M KCN with a spectrofluorophotometer (Fluoroskan Ascent FL, Lab Systems, Germany) at the excitation/emission wavelengths of 485 and 538 nm. Then, IFNα solution (1 mg/mL in PBS, pH 7.4) at various feed molar ratios of 20, 50, 100, and 200 to a single AuNP was added to the HA−AuNP (or AuNP) solution. After incubation at room temperature with mild stirring for 12 h, HA−AuNP/IFNα complex was purified by centrifugation at 20000*g* for 20 min twice and finally redispersed in PBS (pH 7.4). The number of IFNα molecules in the AuNP-based IFNα complexes was determined by human IFNα ELISA of diluted supernatant after centrifugation following the manufacturer's protocol. For further confirmation of the number of IFNα molecules in the AuNP-based IFNα complexes, IFNα was labeled with FITC at one molar ratio following the manufacturer's protocol and dialyzed against PBS (pH 7.4). FITC-IFNα was immobilized onto the surface of HA−AuNP (or AuNP) as described above. After purification by centrifugation, the fluorescence intensity of the supernatants and the AuNP-based IFNα complex solutions after etching in 0.2 M KCN was measured with the spectrofluorophotometer to determine the IFNα content in the AuNP-based IFNα complexes using a standard calibration curve of FITC-IFNα.

Characterization of HA−AuNP/IFNα Complex. The formation of HA−AuNP/IFNα (AuNP/IFNα) complex was analyzed with a UV−vis spectrophotometer (S-3100, Scinco Co., Seoul, Korea). The hydrodynamic diameter of AuNP-based IFNα complexes was determined by DLS (n = 3, Zetasizer Nano, Malvern Instrument Co., UK). For the TEM analysis, each 10 μL drop of the AuNP-based IFNα complex solutions was placed on a 300 mesh copper grid with a carbon film, air-dried, and analyzed with a TEM operating at 300 kV. The interaction between AuNP and IFNα was investigated by a releasing test of IFNα from the AuNP-based IFNα complexes in the presence of chemical reagents known to disrupt specific interactions. HA−AuNP/IFNα (or AuNP/IFNα) complex was treated with 1 M $MgCl_2$ solution, 1% Tween 20 solution, or a combined solution of the two agents with mild stirring for 3 h. After centrifugation at 20000*g* for 20 min, the supernatant was diluted with PBS (pH 7.4) and the amount of

released IFNα was determined with human IFNα ELISA kits. The serum stability of AuNP-based IFNα complexes was assessed after incubation with 2 mg/mL of BSA. A 100 μL amount of each sample was collected at predetermined time intervals, immediately centrifuged at 20000*g* for 20 min, and stored at 4 °C. The amount of released IFNα was determined with human IFNα ELISA kits. Then, the secondary structure of AuNP-based IFNα complexes was analyzed by CD spectroscopy. CD spectra of IFNα, HA−AuNP/IFNα complex, and released IFNα from the HA−AuNP/IFNα complex after treatment with the mixed solution of 1 M $MgCl_2$ and 1% Tween 20 in PBS (pH 7.4) were obtained with a UV spectrophotometer (JASCO J-715, Essex, UK) at 25 °C over the range 200−250 nm under a nitrogen atmosphere. A quartz cuvette with a path length of 2 mm was used, and the data were acquired at 0.2 mm intervals with a response time of 1 s. Each spectrum was subtracted by the spectrum of PBS, and the residual ellipticity was calculated as an average of three scans.

***In Vitro* Biological Activity of HA−AuNP/IFNα Complex.** The human Daudi cell line was maintained in RPMI 1640 media supplemented with 10 vol % fetal bovine serum (FBS) and 10 IU/mL of antibiotics (penicillin). The cells were resuspended at a concentration of 4×10^5 cells/mL in assay media, and 50 μL of the cell suspension containing 2×10^4 cells was seeded on the flat bottom of a 96-well tissue culture plate. Serial dilutions of protein samples were prepared in the assay media, and 50 μL of the diluted protein samples was added to the test wells in triplicate. The plates were incubated at 37 °C in a humidified 5% CO_2 tissue culture incubator for 4 days. Then, 20 μL of Cell Titer 96 AQueous One Solution Reagent was added to each well, and the plates were incubated at 37 °C for 2 h. The absorbance was measured at 490 nm using a microplate reader (EMax, Molecular Devices, CA, USA). After incubation for 4 days, the untreated control was used to calculate the growth inhibition (%). The stability of IFNα and AuNP-based IFNα complexes in human serum was assessed by the same antiproliferation assay using Daudi cells after incubation with human serum at an IFNα concentration of 100 μg/mL at 37 °C for 4 days.

Quantification of IFNα Accumulated in the Tissue. Female Balb/c mice at an age of 5 weeks weighing approximately 20 g were housed under a standard condition of a 12 h light/dark cycle with free access to food and water throughout the study period. The mice were divided into six treatment groups as follows: PBS as a control, IFNα, PEG-Intron, HA−AuNP, AuNP/IFNα 120, and HA−AuNP/IFNα 110 complexes. Each group received a single intravenous injection of the samples at an IFNα dose of 0.5 mg/kg *via* a 26-gauge needle. The dose of HA−AuNP was the same as that of the HA−AuNP in HA−AuNP/IFNα 110 complex. Three mice in each group were sacrificed 4 h, 1 day, 3 days, or 7 days postinjection. A syringe filled with PBS was inserted into the left ventricle, and the right ventricle was cut open for drainage at the same time. PBS was perfused into the heart slowly but constantly. After most of the blood was flushed out, the liver, spleen, kidney, and lung tissues were collected and flash-frozen. To determine the IFNα content accumulated in various organs, the dissected tissue (0.1 g) was homogenized in 1 mL of RIPA buffer as a lysis buffer, maintained at 4 °C for 3 h to recover the IFNα-bound AuNP, and centrifuged at 14 000 rpm and 4 °C for 15 min. The total protein concentration in the supernatant was determined by the BCA protein assay. The IFNα concentration in the supernatant was analyzed with human IFNα ELISA kits.

Quantification of Au Accumulated in the Tissue. As described above, female Balb/c mice at an age of 5 weeks weighing approximately 20 g received a single intravenous injection of PBS as a control, AuNP/IFNα 120, and HA−AuNP/IFNα 110 complexes at an IFNα dose of 0.5 mg/kg. The dose of HA−AuNP was the same as that of the HA−AuNP in HA−AuNP/IFNα 110 complex. After 1 day, the mice were sacrificed and most of the blood was flushed out. The dissected organ samples were dried and weighed. The Au^{3+} content was determined by ICP-MS. The organ samples were dissolved in 5 mL of freshly prepared aqua regia with heating until the solution became transparent. After evaporation, 1 mL of 50% HCl and 1 mL of 50% HNO_3 were added and diluted to a final volume of 10 mL with water. The samples were analyzed by ICP-MS (Thermo Xseries II, Thermo scientific, Soeul, Korea).

Hepatocellular Distribution by ICP-MS. As described above, Balb/c mice at an age of 5 weeks weighing approximately 20 g received a single intravenous injection of AuNP/IFNα 120, HA−AuNP, and HA−AuNP/IFNα 110 complexes. Parenchymal and non-parenchymal cells were isolated from the liver by the collagenase perfusion two-step method. Under ether anesthesia, a midline incision was made in the abdomen of the mice. The portal vein was cannulated with a cutdown tube. The liver was perfused *in situ* with Ca^{2+}-free Hanks' balanced salt (HBS) buffer containing 0.2 vol % ethylene glycol tetraacetic acids and subsequently with HBS buffer containing 1.3 mM $CaCl_2$, 0.015 wt % collagenase, and 0.001 wt % DNase at 37 °C. Immediately after the excision, the liver was minced and suspended in HBS solution containing 0.005 wt % collagenase and 0.001 wt % DNase, and then filtered through a mesh. The cell suspension was centrifuged at 50*g* for 2 min. The obtained pellet was used for isolating parenchymal cells, and the supernatant was used to isolate non-parenchymal cells. The resulting cell suspension was subsequently centrifuged at 400*g* and 4 °C for 10 min. After washing, the isolated cells were resuspended in a staining medium of PBS supplemented with 2 vol % FBS and 1 wt % antibiotics and then incubated with FITC-conjugated mouse anti-CD146 at room temperature for 2 h. The cells were washed with staining medium twice prior to the analysis with a FACS Calibur flow cytometer (BD Biosciences, San Jose, CA, USA). The isolated parenchymal cells were resuspended and recentrifuged twice. The Au^{3+} content was determined by ICP-MS.

TEM for the Hepatocellular Distribution. For the TEM analysis, female Balb/c mice at an age of 5 weeks weighing approximately 20 g received a single intravenous injection of HA−AuNP/IFNα 110 complex at an IFNα dose of 2.5 mg/kg *via* a 26-gauge needle. After 1 day, the mice were sacrificed and most of the blood was flushed out. The dissected liver tissue was fixed with 2% glutaraldehyde and 4% formaldehyde in PBS overnight, and rinsed with 0.1 M cacodylate buffer. Postfixation was performed for 100 min in 1% osmium tetroxide at 4 °C. After several washing steps with 0.1 M cacodylate buffer, the sample was embedded in agarose and dehydrated in a graded series of ethanol (70, 80, 90, 95, and 100 vol %). Then, the sample was embedded in Epon. Ultrathin sections with a thickness of *ca.* 70 nm were imaged with a TEM (JEM-1011, JEOL Ltd., Tokyo, Japan).

Quantification of OAS1 Expression Levels in the Liver Tissue. Female Balb/c mice at an age of 5 weeks weighing approximately 20 g were treated with PBS as a control, IFNα, PEG-Intron, HA−AuNP, AuNP/IFNα 120, HA−AuNP/IFNα 75, and HA−AuNP/IFNα 110 complexes. Each group received a single intravenous injection of the samples at an IFNα dose of 0.5 mg/kg *via* a 26-gauge needle. After the mice were sacrificed 7 days postinjection, the protein was extracted from the liver tissue as described above. The total protein concentration was determined by the BCA protein assay. The proteins were separated by sodium dodecyl sulfate-polyacrylamide gel electrophoresis (SDS-PAGE) and then transferred to a nitrocellulose membrane by wet blotting at a constant current of 1150 mA for 90 min. The membrane was blocked in 5% skim milk at room temperature for 1 h and then incubated with a rabbit anti-OAS1 polyclonal antibody with a dilution of 1/300 at 4 °C overnight. Then, the membrane was washed and incubated with horseradish peroxidase-conjugated goat anti-rabbit IgG with a dilution of 1/5000 at room temperature for 2 h. The signal was detected by exposing the membrane to X-ray for 10 min after mixing with ECL solution. The density of each band was quantified by densitometric analysis using Image J software and normalized by GAPHD band density.

Statistical Analysis. The data are expressed as means ± standard deviation from several separate experiments. Statistical analysis was carried out *via t*-test using SigmaPlot 10.0 software, and a value of $^{**}p < 0.01$ was considered statistically significant.

Conflict of Interest: The authors declare no competing financial interest.

Acknowledgment. This work was supported by the Converging Research Center Program through the National Research Foundation of Korea (NRF) funded by the Ministry of Education, Science and Technology (2009-0081871). This study was also

supported by Midcareer Researcher Program through an NRF grant funded by the MEST (No. 2012R1A2A2A06045773).

Supporting Information Available: Additional figures as discussed in the text. This material is available free of charge *via* the Internet at http://pubs.acs.org.

REFERENCES AND NOTES

1. Ghosh, P.; Han, G.; De, M.; Kim, C. K.; Rotello, V. M. Gold Nanoparticles in Delivery Applications. *Adv. Drug Delivery Rev.* **2008**, *60*, 1307–1315.
2. Thakor, A. S.; Jokerst, J.; Zavaleta, C.; Massoud, T. F.; Gambhir, S. S. Gold Nanoparticles: A Revival in Precious Metal Administration to Patients. *Nano Lett.* **2011**, *11*, 4029–4036.
3. Giljohann, D. A.; Seferos, D. S.; Daniel, W. L.; Massich, M. D.; Patel, P. C.; Mirkin, C. A. Gold Nanoparticles for Biology and Medicine. *Angew. Chem., Int. Ed.* **2010**, *49*, 3280–3294.
4. Lee, M. Y.; Park, S. J.; Park, K.; Kim, K. S.; Lee, H.; Hahn, S. K. Target-Specific Gene Silencing of Layer-by-Layer Assembled Gold-Cysteamine/siRNA/PEI/HA Nanocomplex. *ACS Nano* **2011**, *5*, 6138–6147.
5. Dykman, L.; Khlebtsov, N. Gold Nanoparticles in Biomedical Applications: Recent Advances and Perspectives. *Chem. Soc. Rev.* **2012**, *27*, 2256–2282.
6. Verma, A.; Simard, J. M.; Worrall, J. W.; Rotello, V. M. Tunable Reactivation of Nanoparticle-Inhibited Beta-Galactosidase by Glutathione at Intracellular Concentrations. *J. Am. Chem. Soc.* **2004**, *126*, 13987–13991.
7. Liu, C. L.; Wu, H. T.; Hsiao, Y. H.; Lai, C. W.; Shih, C. W.; Peng, Y. K.; Tang, K. C.; Chang, H. W.; Chien, Y. C.; Hsiao, J. K.; *et al.* Insulin-Directed Synthesis of Fluorescent Gold Nanoclusters: Preservation of Insulin Bioactivity and Versatility in Cell Imaging. *Angew. Chem., Int. Ed.* **2011**, *50*, 7056–7060.
8. Kim, B. Y.; Rutka, J. T.; Chan, W. C. Nanomedicine. *N. Engl. J. Med.* **2010**, *363*, 2434–2443.
9. Paciotti, G. F.; Myer, L.; Weinreich, D.; Goia, D.; Pavel, N.; McLaughlin, R. E.; Tamarkin, L. Colloidal Gold: A Novel Nanoparticle Vector for Tumor Directed Drug Delivery. *Drug Delivery* **2004**, *11*, 169–183.
10. Huang, L.; Liu, Y. *In Vivo* Delivery of RNAi with Lipid-Based Nanoparticles. *Ann. Rev. Biomed. Eng.* **2011**, *13*, 507–530.
11. Poon, Z.; Lee, J. B.; Morton, S. W.; Hammond, P. T. Controlling *in Vivo* Stability and Biodistribution in Electrostatically Assembled Nanoparticles for Systemic Delivery. *Nano Lett.* **2011**, *11*, 2096–2103.
12. Oh, E. J.; Park, K.; Kim, K. S.; Kim, J.; Yang, J. A.; Kong, J. H.; Lee, M. Y.; Hoffman, A. S.; Hahn, S. K. Target Specific and Long-Acting Delivery of Protein, Peptide, and Nucleotide Therapeutics Using Hyaluronic Acid Derivatives. *J. Controlled Release* **2010**, *141*, 2–12.
13. Ito, T.; Iida-Tanaka, N.; Niidome, T.; Kawano, T.; Kubo, K.; Yoshikawa, K.; Sato, T.; Yang, Z.; Koyama, Y. Hyaluronic Acid and its Derivative as a Multi-Functional Gene Expression Enhancer: Protection from Non-Specific Interactions, Adhesion to Targeted Cells, and Transcriptional Activation. *J. Controlled Release* **2006**, *112*, 382–388.
14. Ahrens, T.; Assmann, V.; Fieber, C.; Termeer, C.; Herrlich, P.; Hofmann, M.; Simon, J. C. CD44 is the Principal Mediator of Hyaluronic-Acid-Induced Melanoma Cell Proliferation. *J. Invest. Dermatol.* **2001**, *116*, 93–101.
15. Entwistle, J.; Hall, C. L.; Turley, E. A. HA Receptors: Regulators of Signaling to the Cytoskeleton. *J. Cell Biochem.* **1996**, *61*, 569–577.
16. Zhou, B.; Weigel, J. A.; Fauss, L.; Weigel, P. H. Identification of the Hyaluronan Receptor for Endocytosis (HARE). *J. Biol. Chem.* **2000**, *275*, 37733–37741.
17. Kim, K. S.; Hur, W.; Park, S. J.; Hong, S. W.; Choi, J. E.; Goh, E. J.; Yoon, S. K.; Hahn, S. K. Bioimaging for Targeted Delivery of Hyaluronic Acid Derivatives to the Livers in Cirrhotic Mice Using Quantum Dots. *ACS Nano* **2010**, *4*, 3005–3014.
18. Yang, J. A.; Park, K.; Jung, H.; Kim, H.; Hong, S. W.; Yoon, S. K.; Hahn, S. K. Target Specific Hyaluronic Acid-Interferon Alpha Conjugate for the Treatment of Hepatitis C Virus Infection. *Biomaterials* **2011**, *32*, 8722–8729.
19. Chevaliez, S.; Pawlotsky, J. M. Interferon-Based Therapy of Hepatitis C. *Adv. Drug Delivery Rev.* **2007**, *59*, 1222–1241.
20. Thitinan, S.; McConville, J. T. Interferon Alpha Delivery Systems for the Treatment of Hepatitis C. *Int. J. Pharm.* **2009**, *369*, 121–135.
21. Cheng, J. C.; Yeh, Y. J.; Huang, Y. H.; Liang, K. H.; Chang, M. L.; Lin, C. Y.; Yeh, C. T. Hepatic Expression of MxA and OAS1 in an *Ex Vivo* Liver Slice Assay Independently Predicts Treatment Outcomes in Chronic Hepatitis C. *J. Viral. Hepat.* **2012**, *19*, 154–162.
22. Warren, A.; Bertolino, P.; Benseler, V.; Fraser, R.; McCaughan, G. W.; Le Couteur, D. G. Marked Changes of the Hepatic Sinusoid in a Transgenic Mouse Model of Acute Immune-Mediated Hepatitis. *J. Hepatol.* **2007**, *46*, 239–246.
23. Carillo, M. C.; Alvarez Mde, L.; Quiroga, A. D. Interferon Alfa-2b Triggers Transforming Growth Factor-Beta-Induced Apoptosis on Preneoplasticliver. *Ann. Hepatol.* **2006**, *5*, 244–250.
24. Lee, K.; Lee, H.; Bae, K. H.; Park, T. G. Heparin Immobilized Gold Nanoparticles for Targeted Detection and Apoptotic Death of Metastatic Cancer Cells. *Biomaterials* **2010**, *31*, 6530–6536.
25. Schwarzenbach, M. S.; Reimann, P.; Thommen, V.; Hegner, M.; Mumenthaler, M.; Schwob, J.; Güntherodt, H. J. Interferon Alpha-2a Interactions on Glass Vial Surfaces Measured by Atomic Force Microscopy. *PDA J. Pharm. Sci. Technol.* **2002**, *56*, 78–89.
26. Calzolai, L.; Franchini, F.; Gilliland, D.; Rossi, F. Protein-Nanoparticle Interaction: Identification of the Ubiquitin-Gold nanoparticle Interaction Site. *Nano Lett.* **2010**, *10*, 3101–3205.
27. Mukherjee, P.; Bhattacharya, R.; Bone, N.; Lee, Y. K.; Patra, C. R.; Wang, S.; Lu, L.; Secreto, C.; Banerjee, P. C.; Yaszemski, M. J.; *et al.* Potential Therapeutic Application of Gold Nanoparticles in B-Chronic Lymphocytic Leukemia (BCLL): Enhancing Apoptosis. *J. Nanobiotechnol.* **2007**, *5*, 4.
28. Beilharz, M. W.; Nisbet, I. T.; Tymms, M. J.; Hertzog, P. J.; Linnane, A. W. Antiviral and Antiproliferative Activities of Interferon-Alpha 1: the Role of Cysteine Residues. *J. Interferon Res.* **1986**, *6*, 677–685.
29. Lacerda, S. H.; Park, J. J.; Meuse, C.; Pristinski, D.; Becker, M. L.; Karim, A.; Douglas, J. F. Interaction of Gold Nanoparticles with Common Human Blood Proteins. *ACS Nano* **2010**, *4*, 365–379.
30. Tsai, D. H.; Delrio, F. W.; Keene, A. M.; Tyner, K. M.; Maccuspie, R. I.; Cho, T. J.; Zachariah, M. R.; Hackley, V. A. Adsorption and Conformation of Serum Albumin Protein on Gold Nanoparticles Investigated Using Dimensional Measurements and *in Situ* Spectroscopic Methods. *Langmuir* **2011**, *27*, 2464–2477.
31. Slocik, J. M.; Govorov, A. O.; Naik, R. R. Plasmonic Circular Dichroism of Peptide-Functionalized Gold Nanoparticles. *Nano Lett.* **2011**, *11*, 701–705.
32. Petricoin, E. F.; Ito, S.; Williams, B. L.; Audet, S.; Stancato, L. F.; Gamero, A.; Clouse, K.; Grimley, P.; Weiss, A.; Beeler, J. Antiproliferative Action of Interferon-Alpha Requires Components of T-Cell-Receptor Signalling. *Nature* **1997**, *390*, 629–632.
33. Lauer, G. M.; Walker, B. D. Hepatitis C Virus Infection. *N. Engl. J. Med.* **2001**, *345*, 41–52.
34. Rebouillat, D.; Hovanessian, A. G. The Human 2′,5′-Oligoadenylate Synthetase Family: Interferon-Induced Proteins with Unique Enzymatic Properties. *J. Interferon Cytokine Res.* **1999**, *19*, 295–308.